

## Circulating Myeloid-derived Suppressor Cells Facilitate Invasion of Thyroid Cancer Cells by Repressing miR-486-3p

Li Chen,<sup>1</sup> Li Xiong,<sup>1</sup> Shubing Hong,<sup>1</sup> Jin Li,<sup>2</sup> Zijun Huo,<sup>1</sup> Yudong Li,<sup>3,4</sup> Shuwei Chen,<sup>3,4</sup> Quan Zhang,<sup>3,4</sup> Ruiying Zhao,<sup>5</sup> Julian A. Gingold,<sup>6</sup> Xiaonan Zhu,<sup>7</sup> Weiming Lv,<sup>8</sup> Yanbing Li,<sup>1</sup> Shuang Yu,<sup>1</sup> and Haipeng Xiao<sup>1</sup>

<sup>1</sup>Department of Endocrinology, The First Affiliated Hospital of Sun Yat-Sen University, Guangzhou 510080, China; <sup>2</sup>Department of Geriatrics, The First Affiliated Hospital of Sun Yat-Sen University, Guangzhou 510080, China; <sup>3</sup>Department of Head and Neck Surgery, Sun Yat-Sen University Cancer Center, Guangzhou 510060, China; <sup>4</sup>State Key Laboratory of Oncology in South China, Collaborative Innovation Center of Cancer Medicine, Guangzhou 510060, China; <sup>5</sup>Department of Integrative Biology and Pharmacology, McGovern Medical School, The University of Texas Health Science Center at Houston, Houston, Texas 77030; <sup>6</sup>Department of Obstetrics & Gynecology and Women's Health, Einstein/Montefiore Medical Center, New York, New York 10461; <sup>7</sup>Zhongshan School of Medicine, Sun Yat-Sen University, Guangzhou 510080, China; and <sup>8</sup>Department of Breast and Thyroid Surgery, The First Affiliated Hospital of Sun Yat-sen University, Guangzhou 510080, China

**ORCID numbers:** 0000-0001-7242-760X (Y. Li); 0000-0002-4188-336X (H. Xiao).

**Background:** Myeloid-derived suppressor cells (MDSCs) have become increasingly recognized as facilitators of tumor development. However, the role of MDSCs in papillary thyroid carcinoma (PTC) progression has not been clearly explored.

**Objective:** We aimed to evaluate the levels and function of circulating MDSCs in PTC.

**Methods:** The proportion of circulating polymorphonuclear (PMN)-MDSCs and mononuclear-MDSCs from patients with PTC or benign thyroid nodules and healthy controls was measured using flow cytometry. For immunosuppressive activity analysis, sorted circulating MDSCs were cocultured with CD3/CD28-costimulated T lymphocytes and the proliferation of T cells was determined. PTC cell lines (TPC-1 and BC-PAP) were cocultured with PMN-MDSCs, and the effects on cell migration, invasion, proliferation, and apoptosis were evaluated. The differential expressed microribonucleic acids (RNAs) and messenger RNAs and their function were also explored in TPC-1 cells cocultured with or without PMN-MDSCs.

**Results:** PMN-MDSCs were increased in peripheral blood mononuclear cells of patients with PTC. Circulating PMN-MDSCs displayed strong T cell suppressive activity. PTC cells demonstrated enhanced invasive capabilities *in vitro* and *in vivo* when cocultured with sorted PMN-MDSCs. PMN-MDSCs decreased expression of miR-486-3p and activated nuclear factor kappa B2 (NF- $\kappa$ B2), a direct target of miR-486-3p. Rescue of miR-486-3p diminished the cell migration and invasion induced by PMN-MDSCs.

**Conclusion:** Collectively, our work indicates that circulating PMN-MDSCs promote PTC progression. By suppressing miR-486-3p, PMN-MDSCs promote the activity of the NF- $\kappa$ B2 signaling pathway, resulting in accelerated invasion of PTC cells, which may provide new

ISSN Print 0021-972X ISSN Online 1945-7197

Printed in USA

© Endocrine Society 2020. All rights reserved. For permissions, please e-mail: journals.permissions@oup.com

Received 13 February 2020. Accepted 30 May 2020.

First Published Online 3 June 2020.

Corrected and Typeset 27 June 2020.

Abbreviations: DMEM, Dulbecco's modified Eagle's medium; FDR, false discovery rates; GAPDH, glyceraldehyde 3-phosphate dehydrogenase; GO, gene ontology; H&E, hematoxylin and eosin; IFN, interferon; M, mononuclear; MDSC, myeloid-derived suppressor cell; miRNA, microribonucleic acid; NF- $\kappa$ B2, nuclear factor kappa B2; PMBC, peripheral blood mononuclear cell; PMN, polymorphonuclear; PTC, papillary thyroid carcinoma; SD, standard deviation; TBST, tris buffered saline and tween; TME, tumor microenvironment; TNF, tumor necrosis factor; UTR, untranslated region.

therapeutic strategies for treatment of thyroid cancer. (*J Clin Endocrinol Metab* 105: 2704–2718, 2020)

**Key Words:** myeloid-derived suppressor cells, papillary thyroid carcinoma, miR-486-3p, tumor invasion

The incidence and prevalence of thyroid cancer has been rapidly increasing over the past 20 years (1). Most of this increase has been attributed to papillary thyroid carcinoma (PTC), the most common histologic thyroid cancer subtype (1). PTC shows a relatively low mortality rate in its early stages (overall 5-year survival rate of 97%) (1, 2). However, approximately one-third of PTC patients ultimately develop extracapsular extension and lymph node metastasis (3), and advanced-stage PTC carries a significantly higher risk of recurrence and a poorer prognosis (4). Therefore, exploring the progression and metastasis of PTC is of great importance for improving the prognosis of PTC.

Tumor cells and the host immune system interact within the tumor microenvironment (TME). The TME comprises infiltrating immune cells, extracellular matrix, and tumor-associated fibroblasts and cytokines. There is overwhelming evidence that the TME plays a pivotal role in tumorigenesis and tumor metastasis (5, 6). Myeloid-derived suppressor cells (MDSCs), a component of the TME, are defined as a heterogeneous group of immature immune cells activated under pathologic conditions. MDSCs are typically divided into 2 major subsets based on their phenotypic and morphologic features: polymorphonuclear (PMN)-MDSCs and mononuclear (M)-MDSCs. Human PMN-MDSCs are defined as CD11b<sup>+</sup>CD14<sup>-</sup>CD15<sup>+</sup> or CD11b<sup>+</sup>CD14<sup>-</sup>CD66b<sup>+</sup> and M-MDSCs as CD11b<sup>+</sup>CD14<sup>+</sup>HLA-DR<sup>-low</sup>CD15<sup>-</sup> (7, 8). MDSCs mediate their potent immunosuppressive effects, including facilitating escape from immune surveillance, mainly by suppressing T cell activation and proliferation (9). Ample evidence also supports a close correlation between MDSC accumulation and tumor vasculogenesis, metastasis, as well as cancer cell stemness across multiple cancer types, including hepatocellular carcinoma, breast cancer, ovarian cancer, and pancreatic cancer (10–13).

Previous studies reported elevated proportions of circulating MDSCs in differentiated thyroid carcinoma patients (14). In addition, in a murine orthotopic model of anaplastic thyroid cancer, administration of lenvatinib and anti-PD-1/PD-L1 or BRAF inhibitor and anti-PD-1/PD-L1 combination therapy led to reduced tumor volume and prolonged overall survival (15, 16). This combination therapy was also associated with a significant decrease in the proportion of

MDSCs, raising the tantalizing possibility that MDSCs may represent potential treatment targets. However, further study is necessary to confirm the biologic functions and roles of circulating MDSCs in PTC, particularly in humans.

Microribonucleic acids (miRNAs) are a conserved class of small noncoding RNAs (approximately 22 nucleotides in length) that negatively regulate target gene expression (17). Recent studies have not only indicated that miRNAs emerged as important regulators of MDSCs biology, but also MDSCs can modulate miRNA expression during carcinogenesis (18). MDSCs can induce miR-101 overexpression and promote cancer stemness (12). Moreover, MDSC release of miR-126a has been shown to facilitate lung metastasis (19). In this study, we aimed to identify the proportion of circulating MDSCs in PTC patients and explore the molecular mechanisms of MDSCs in regulating PTC cell migration and invasion, including transcriptional and miR regulatory changes.

## Materials and Methods

### Patients and samples

Peripheral blood samples from 101 patients were collected at the First Affiliated Hospital of Sun Yat-sen University and Sun Yat-sen University Cancer Center (Guangzhou, China) from October 2017 to July 2019. The pathologic diagnosis of PTC was performed according to the World Health Organization criteria (20). Among the 101 patients, 64 patients (mean age, 41.56 years; range 17–71) with histologically confirmed PTC and 35 patients (mean age, 42.28 years; range 23–67) with benign thyroid nodules were enrolled in the current study; 2 PTC patients were excluded since 1 had concurrent breast cancer and the other colorectal cancer. All samples collected from patients with PTC or benign thyroid nodules were obtained prior to surgery or radioactive iodine treatment. All patients subsequently underwent an excisional surgical procedure that was used to provide a final histologic diagnosis. The specific surgery performed varied across patients and included lobectomy, total thyroidectomy, and total thyroidectomy with lymph node dissection. Individuals without history of cancer, thyroid nodules, autoimmune disease, or infectious disease were selected as healthy controls. Three individuals with hepatitis were excluded. Eventually, a total of 50 healthy individuals (mean age, 44.63 years; range 17–66) were included. Written informed consent was acquired from all participants before blood sample collection. This study was approved by the Institutional Research Ethics Committee of Sun Yat-sen University.

## Cell culture and transfection

The human PTC cell lines TPC-1 and BC-PAP were provided as generous gifts from Professor Haixia Guan of China Medical University. TPC-1 and BC-PAP cell lines were authenticated using short tandem repeat analysis. HEK293T cells were purchased from the American Type Culture Collection (ATCC, VA, USA). Cells were cultured in Dulbecco's modified Eagle's medium (DMEM) (Invitrogen, CA, USA) supplemented with 10% fetal bovine serum and penicillin/streptomycin (Gibco, MD, USA). Cells were incubated at 37°C under humidified conditions with 5% CO<sub>2</sub>. For cell coculture, the PTC cell lines were cultured with PMN-MDSCs in a transwell system at a 2:1 ratio. TPC-1 and BC-PAP were added to the lower chambers and maintained for 24 hours, followed by addition of PMN-MDSCs to the upper chambers and incubation for another 48 hours. For the control group, TPC-1 and BC-PAP were added to the lower chambers, and after 24 hours culture medium was added to the upper chamber and maintained for 48 hours.

miR-486-3p mimics (50 nM), miR-486-3p inhibitor (100 nM) and corresponding negative controls (RiboBio, Guangzhou, China) were transfected into TPC-1 cells. Stable cell lines were established by transducing TPC-1 cells with a lentivirus-expressing miR-486-3p precursor (HmiR0130-MR03) or miR-486-3p inhibitor (antagomiR-486-3p) (HmiR-AN0 522-AM03) (GeneCopoeia, Guangzhou, China). Cells were transfected with a GV657 vector (Shanghai GeneChem, Shanghai, China) encoding human NF-κB2 or the control empty vector, NF-κB2 siRNAs (RiboBio) and control siRNA (RiboBio) using Lipofectamine 3000 (Invitrogen).

## PBMC isolation and flow cytometric analysis

Peripheral blood mononuclear cells (PBMCs) from fresh blood samples were isolated by Ficoll centrifugation. Single cell suspensions were stained with antihuman CD11b-FITC (clone: ICRF44), CD15-PE (clone: HI98), CD14-PE-Cy7 (clone: 61D3), CD3-APC (clone: UCHT1) (eBioscience, CA, USA), HLA-DR-APC (clone: TU36), CD4-BV421 (clone: RM4-5), and CD8-BV605 (clone: 53–6.7) (BD Pharmingen, CA, USA) and their corresponding isotype antibodies. Stained cells were resuspended in 100 μL for analysis on an Aurora flow cytometer (Cytex Biosciences, CA, USA). Isolation of MDSCs and T cells from human PBMCs was performed on a MoFlo Astrios EQs cell sorter (Beckman Coulter, USA). The CD11b<sup>+</sup>CD15<sup>+</sup>CD14<sup>-</sup>, CD11b<sup>+</sup> CD14<sup>+</sup>CD15<sup>-</sup>, and CD3<sup>+</sup> population was gated as PMN-MDSCs, M-MDSCs and T cells. Data were collected and analyzed using FlowJo software (Tree Star, Ashland, USA).

## T-cell proliferation assay

Each PBMC sample was isolated from each patient and stained with CD3-APC, CD11b-FITC, CD15-PE, and CD14-PE-Cy7 for cell sorting to isolate CD3<sup>+</sup> T cells, PMN-MDSCs (marked as CD11b<sup>+</sup>CD15<sup>+</sup>CD14<sup>-</sup>) and M-MDSCs (marked as CD11b<sup>+</sup> CD14<sup>+</sup>CD15<sup>-</sup>). After isolation, CD3<sup>+</sup> T cells were labeled with CFSE (5, 6 carboxyfluorescein diacetate, succinimidylester) (2 μM) (Invitrogen), stimulated with antihuman CD3 (5 μg/mL) and soluble antihuman CD28 (1 μg/mL) antibody (eBioscience) and cultured alone or with MDSCs at different ratios (1:2–8). After 96 hours, cells were stained with CD4-BV421 and CD8-BV605 antibodies and

analyzed by flow cytometry. Culture supernatants were collected to measure interferon (IFN)-γ concentrations using an enzyme-linked immunosorbent assay kit (eBioscience) following the manufacturer's instructions.

## Transwell assay

After cell transfection or cell coculturing, PTC cell lines (TPC-1 and BC-PAP) were then seeded following trypsinization in the upper chambers. For the invasion assay, chambers were precoated with diluted Matrigel (Corning). A 100-μL bolus of the PTC tumor cell suspension containing 0.5% fetal bovine serum at a density of  $5 \times 10^4$  cells/mL was added to the upper chambers; 500 μL of DMEM containing 10% fetal bovine serum was added to the lower chambers. After 24 hours of incubation, cells were fixed with 4% paraformaldehyde and then stained with crystal violet solution. The migratory and invasive cells were counted in 5 randomly selected low-power fields under an inverted microscope (Leica, Germany).

## Wound-healing assay

PTC cell lines (TPC-1 and BC-PAP) were diluted and  $5 \times 10^4$  cells were added into each well of the Ibidi 2-Well Culture Insert system (Ibidi, Martinsried, Germany) in a 12-well plate. After 24 hours, the insert was gently removed and the cells cultured in serum-free DMEM for another 24 hours. Scratch wounds were photographed in the same position at 0 hours and 24 hours, respectively.

## Cell proliferation assay

Cell proliferation was determined by MTS (3-(4,5-dimethylthiazol-2-yl)-5-(3-carboxymethylthioxyphenyl)-2-(4-sulfophenyl)-2H-tetrazolium) reagent. Since MTS is bioreduced by cells into a colored formazan product that is soluble in cell culture medium, the absorbance is proportional to the number of cells. A total of 1000 to 2000 PTC cell lines (TPC-1 and BC-PAP) were seeded in a 96-well plate and cultured for 24 hours, 36 hours, and 72 hours. After the specified time interval, MTS reagent (Promega, WI, USA) was added to each well and incubated at 37°C for 4 hours. Cell proliferation was determined by measuring the absorbance at 450 nm using a microboard reader (Bio-Rad, California, USA).

## Cell cycle and apoptosis analysis

For cell cycle analysis, cells were washed with phosphate-buffered saline, fixed in 70% ethanol overnight and then stained with propidium iodide (BD Pharmingen). The apoptosis analysis was determined using an Annexin V-APC/PI Apoptosis Kit (KeyGEN BioTECH, Nanjing, China). Stained cells were detected by flow cytometry. Cell cycle distributions were assessed using ModFit LT software and the percentage of apoptotic cells was determined with FlowJo software.

## Quantitative real-time PCR

Total RNA of cells was extracted using TRIzol Reagent (Invitrogen) and RNA concentration was determined by Nano Drop 2000C (Thermo Scientific, CA, USA). miRNAs were reverse transcribed using a Ribo™ Reverse Transcription Kit (RiboBio) with the miRNA-specific RT primer (RiboBio). mRNAs were reverse transcribed using PrimeScript™ RT reagent Kit (Perfect Real Time) (Takara,

Dalian, China). Polymerase chain reactions (PCR) were performed using TB Green® Premix Ex Taq™ II (Tli RNaseH Plus) (TaKaRa) in a LightCycler 480 (Roche Diagnostics, Pleasanton, CA). U6 and glyceraldehyde 3-phosphate dehydrogenase (GAPDH) were used as control. The qRT-PCR primers employed were the following: NF-κB2 forward: 5'-TGAGCAGCATTTAGCAGCAAG-3', NF-κB2 reverse: 5'-AGGGCCTGAGAAGGACACC-3'; RELB forward: 5'-GCGAGGCAGGTACG TGAAA-3', RELB reverse: 5'-CGACAAGGTGCAGAAAGAGG-3'; GAPDH forward: 5'-GGACCTGACCTGCCGTCTAG-3', GAPDH reverse: 5'-GTAGCCCAGGATGCCCTT GA-3'. Relative expression was calculated by  $2^{-\Delta\Delta Ct}$  method.

### Western blot analysis

RIPA lysis buffer (Thermo Scientific) was used to extract protein from cells and the Pierce™ BCA Protein Assay Kit (Thermo Scientific) was used to measure the protein concentration. Equal amounts of protein sample were separated by 10% sodium dodecyl sulfate polyacrylamide gel electrophoresis and transferred to polyvinylidene fluoride membrane (Millipore, MA, USA). After blocking with 5% bovine serum albumin, membranes were incubated with rabbit anti-NF-κB2 (Cell Signaling Technology, MA, USA), anti-RelB (Proteintech, IL, USA), and anti-GAPDH (Proteintech) at a 1:1000 dilution overnight at 4°C. After washing with tris buffered saline and tween (TBST), the bands were then incubated with the secondary antibody of conjugated antirabbit horseradish peroxidase (Cell Signaling Technology) at room temperature for 2 hours. Bands were exposed by Immobilon Western Chemiluminescent horseradish peroxidase substrate (Millipore) and the signals were detected with an Amersham Imager 600 (GE Healthcare Life Sciences, USA).

### Dual luciferase activity assay

The NF-κB2 wild-type 3' (untranslated region) UTR sequence (NF-κB2-wt) and a mutated NF-κB2 3' UTR (NF-κB2-mut) were cloned into the 3' UTR region of the renilla luciferase gene in the psiCheck2 vector (Promega). HEK293T cells were seeded in 24-well plates. miR-486-3p mimics or miR-NC and NF-κB2-wt or NF-κB2-mut were cotransfected into HEK293T cells. Forty-eight hours after transfection, a Dual Luciferase Reporter Assay System (Promega) was used to detect firefly and renilla luciferase activity using Infinite F500 (Tecan, Switzerland). Firefly luciferase activity was used as a normalized control.

### Tumor metastasis assay in vivo

Male 5-week-old BALB/c nude mice were purchased from GemPharmatech (Nanjing, China) and maintained in a specific pathogen-free facility of Sun Yat-sen University. After coculture with or without PMN-MDSCs for 48 hours, TPC-1 cells were used to seed mice for lung metastasis models. TPC-1 cells were diluted to  $1 \times 10^6/200 \mu\text{L}$  with phosphate-buffered saline and cell suspensions were intravenously injected into the mice. At 5 weeks post tumor injection, the mice were killed and lung tissues were removed, followed by hematoxylin and eosin (H&E) staining. Lung tissues were fixed in 4% paraformaldehyde and cut into 4- $\mu\text{m}$ -thick sections after being embedded in paraffin. The sections were stained with H&E to evaluate lung metastasis. The animal experiments

were approved by the Animal Ethics Committee of the First Affiliated Hospital of Sun Yat-sen University.

### RNA-sequencing data analysis.

The cDNA libraries were constructed for each RNA sample using the TruSeq Stranded mRNA Library Prep Kit (Illumina, USA) according to the manufacturer's instructions. The miRNA library was prepared from total RNA using the NEBNext Small RNA Library Prep Set for Illumina (NEB) according to the manufacturer's instructions.

Before read mapping, clean reads were obtained from the raw reads by removing the adaptor sequences and low-quality reads. The clean reads were then aligned to the human genome (GRCh38, NCBI) using Hisat2. HTseq was used to calculate gene counts and the RPKM method used to determine relative gene expression. The clean reads from the miRNA library were mapped to the human miRNA database (miRBase v22.0) to compute miRNA expression. The EdgeR package was used to identify differentially expressed RNAs with fold change  $>1.5$  or  $<0.67$  with a false discovery rate (FDR)  $<0.05$ . Miranda and RNAhybrid tools were used to predict miRNA targets.

### GO and pathway analysis

Gene ontology (GO) analysis was performed to elucidate the biologic implications of the differentially expressed genes identified in the experiment. We downloaded the GO annotations from NCBI (<http://www.ncbi.nlm.nih.gov/>), UniProt (<http://www.uniprot.org/>) and the Gene Ontology (<http://www.geneontology.org/>). Fisher's exact test was applied to identify significantly enriched GO categories with  $P < .05$ . Pathway analysis was conducted using the KEGG database to identify pathways enriched by Fisher's exact test with  $P < .05$  (21). Data have been deposited in the GEO data repository (accession number GSE140109).

### Statistical analysis

Statistical analyses were performed with SPSS 20.0 and Graphpad Prism v7.00. Results are reported as mean  $\pm$  standard deviation (SD). The significance of differences between 2 groups was assessed by Student's t-test for parametric data and Mann-Whitney U-tests for nonparametric data. The correlation between circulating PMN-MDSCs and CD3<sup>+</sup> CD8<sup>+</sup> T cells was assessed by Pearson's correlation test. Results meeting the  $P < .05$  threshold were considered statistically significant.

## Results

### Expansion of PMN-MDSCs in PTC patients

To determine the potential role of MDSCs in PTC, we compared the MDSC proportions in peripheral blood of patients with PTC or benign thyroid nodules and healthy controls, using the presence of CD11b, HLA-DR, CD14, and CD15 surface markers to define MDSC subsets. Two distinct MDSC populations (CD11b<sup>+</sup>HLA-DR<sup>-low</sup>CD15<sup>+</sup>CD14<sup>-</sup> and CD11b<sup>+</sup>HLA-DR<sup>-low</sup>CD14<sup>+</sup>CD15<sup>-</sup>) were observed

in PTC patients, corresponding to MDSCs derived from PMNs and mononuclear cells, respectively (all supplementary material and figures are located in a digital research materials repository (22)). Morphology of sorted MDSC subsets in PBMC was confirmed by Wright–Giemsa staining (22). Flow cytometric analysis showed that PMN-MDSC proportions in PTC patients were significantly increased compared with those in patients with benign thyroid nodules, which were significantly increased compared with the PMN-MDSC proportions in healthy individuals. In contrast, no changes were observed in the proportion of M-MDSCs among cancer patients, those with thyroid nodules, and healthy patients (Fig. 1A and 1B). Furthermore, the PMN-MDSC proportion was most elevated in patients with more aggressive (TNM Stage III/IV) PTC (Fig. 1C). Thus, these findings support a dose–response relationship between PMN-MDSC levels and increasing thyroid cancer characteristics, with progressively increasing PMN-MDSC fractions from healthy individuals to those with benign thyroid nodules to those with PTC (Table 1).

**MDSCs from PTC patients suppress T cell responses**

Given the known immunosuppressive activity of MDSCs in the context of other cancers (7), we next determined whether circulating MDSCs can dampen T cell immune responses using a T cell proliferation assay. Proliferation of CD8<sup>+</sup> and CD4<sup>+</sup> T cells stimulated by CD3 and CD28 antibodies was inhibited when the T cells were cocultured with PMN-MDSCs isolated from the peripheral blood of cancer patients at a ratio of 2:1 or 4:1 (Fig. 2A–2D). This inhibition of T cell activity by PMN-MDSCs from PTC patient peripheral blood functionally confirms them to be MDSCs. Similar effects were observed for M-MDSCs (22).

T cell exhaustion contributes to immune evasion and is characterized by impaired proliferation capacity and reduced circulating levels of effector cytokines, including IL-2, tumor necrosis factor (TNF)- $\alpha$  and IFN- $\gamma$  (23). We found that the levels of IFN- $\gamma$  decreased in supernatants of cocultured human MDSCs and CD3<sup>+</sup> T cells compared with CD3<sup>+</sup> T cells alone (Fig. 2E). We also evaluated the correlation between the MDSC proportion among PBMCs and the CD8<sup>+</sup> proportion among T cells.

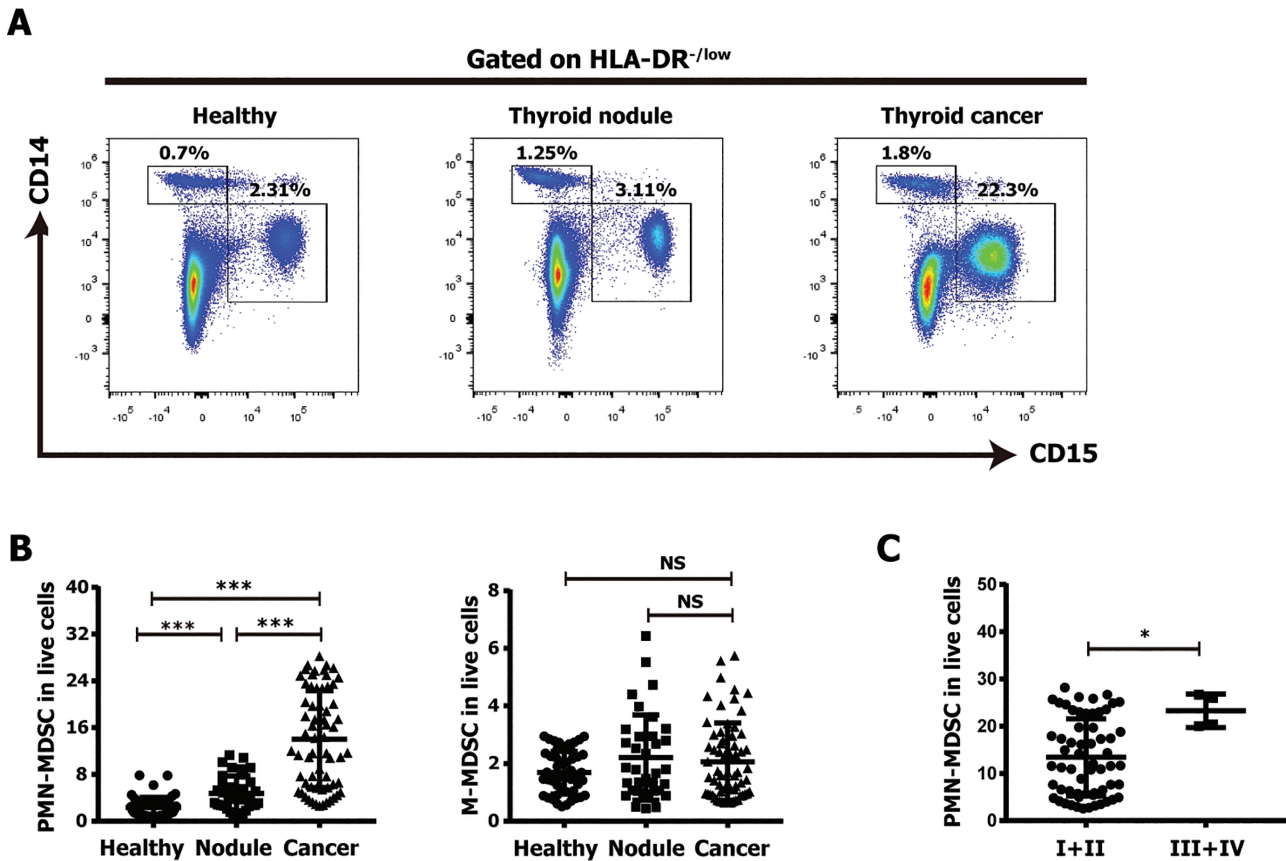


**Figure 1.** Expansion of PMN-MDSCs in patients with PTC. (A) Circulating MDSCs obtained from the PBMC of patients with PTC (n = 64) or a benign thyroid nodule (n = 35) and healthy controls (n = 50) were assessed by flow cytometry. Representative images of flow cytometry from one healthy individual, patient with thyroid nodule and PTC patient are shown. (B) Proportions of PMN-MDSCs and M-MDSCs subsets in the PBMCs in each of the groups, as measured by flow cytometry. (C) Proportions of PMN-MDSCs in PBMC of PTC patients of different TNM stages. Data are presented as mean  $\pm$  SD; \**P* < .05, \*\*\**P* < .001. NS, not significant.

**Table 1. Relationship between proportion of PMN-MDSCs and clinicopathologic characteristics of PTC patients.**

	Number of PTC patients	PMN-MDSCs	P value
Sex			
Male	19 (29.69)	13.55 ± 7.11	.7569
Female	45 (70.31)	14.25 ± 8.78	
Age (years)			
<55	52 (81.25)	12.98 ± 8.08	.0342
≥55	12 (18.75)	18.64 ± 7.79	
Tumor size			
≤2 cm	50 (78.13)	13.09 ± 8.11	.1149
>2 cm	14 (21.87)	17.44 ± 8.23	
Invasion <sup>a</sup>			
Yes	12 (18.75)	18.46 ± 6.13	.0293
No	52 (81.25)	13.02 ± 8.41	
Lymph node metastasis			
Yes	33 (51.56)	14.37 ± 8.65	.7499
No	31 (48.44)	13.7 ± 7.98	
Distant metastasis			
Yes	3 (4.69)	24.35 ± 3.46	.0149
No	61 (95.31)	13.54 ± 8.11	
TMN stage			
I-II	60 (93.75)	13.43 ± 8.14	.0130
III-IV	4 (6.25)	23.27 ± 3.55	

Abbreviation: TMN, Tumor–Nodal–Metastasis stage.

<sup>a</sup>Includes capsular and/or extrathyroidal extension.

The results showed that the PMN-MDSC proportion is strongly negatively correlated with the CD8<sup>+</sup> T cell proportion ( $r = -0.5323$ ;  $P = .0037$ ) (22). Taken together, these findings demonstrated that MDSCs in the peripheral blood of PTC patients display T cell suppressive activity in a dose-dependent manner.

### PMN-MDSC enhanced cell migration and invasion of PTC

Given the significant role of MDSCs in tumorigenesis among various cancer types as well as the clinical and functional relevance of PMN-MDSCs in PTC patients demonstrated in our initial experiments, we next explored the biologic functions of PMN-MDSCs in PTC cells. PMN-MDSCs remarkably increased migration and invasion of both TPC-1 and BC-PAP cell lines compared with PTC lines cultured without PMN-MDSCs (Fig. 3A, 3C, and 3D). Moreover, PTC cells showed increased wound closure rates when cocultured with sorted PMN-MDSCs (Fig. 3B, 3E, and 3F). We also generated a pulmonary metastasis model to investigate the effects of PMN-MDSCs on cancer cell metastasis in vivo. Mice intravenously injected with TPC-1 cells cocultured with PMN-MDSCs developed many more metastatic lung nodules than those injected with TPC-1 cells alone (Fig. 3G and 3H). More tumor regions per low-power field were also visible on H&E staining of

lung tissue (Fig. 3I). It seems that there is no significant effect of MDSCs on cell viability, cell cycle, and apoptosis (22).

Collectively, these results support a role of PMN-MDSCs in promoting PTC cell migration and invasion, both in vitro and in vivo, while highlighting that they have little to no effect on cell growth and apoptosis.

### PMN-MDSCs accelerate invasion and metastasis by suppressing miR-486-3p

miRNAs have been shown to drive human tumorigenesis by affecting differentiation, proliferation, and metastasis of tumor cells (24, 25). To explore whether MDSCs regulate PTC oncogenicity by modulating miRNA expression, miRNA profiling was performed in untreated TPC-1 cells and TPC-1 cells cocultured with PMN-MDSCs sorted from PBMCs of cancer patients. We identified 19 differentially expressed miRNAs in MDSC-conditioned cancer cells, of which 10 were downregulated and 9 were upregulated (Fig. 4A and (22)). The expression alterations of miR-486-3p, miR-146a-3p, miR-146a-5p, miR-200b-3p, miR-486-5p, and miR-152-5p were further confirmed by qRT-PCR (Fig. 4B and (22)). GO analysis of predicted targets of the 19 miRNAs showed enrichment of inflammation-related response genes (Fig. 4C). And the KEGG pathway analysis reveals that these genes were mainly from the NF- $\kappa$ B, PI3K-AKT, and TNF signaling pathways, all of which are recognized to regulate cancer development (Fig. 4D).

Among the validated miRs, miR-486-3p stood out as the most likely regulator of thyroid cancer invasion and metastasis. miR-486-3p is known to negatively regulate most genes of the NF- $\kappa$ B and TNF signaling pathways, which are essential for MDSCs activation (26), while the other identified dysregulated miRNAs have little known effect on these pathways. Based on these evidences, we hypothesized that miR-486-3p plays a vital role in mediating the function of PMN-MDSCs in thyroid cancer. To confirm this, we next rescued miR-486-3p expression in cells co-cultured with PMN-MDSCs and evaluated cell invasion and metastasis. Overexpression of miR-486-3p by transfection with miR-486-3p mimics repressed MDSCs-induced migration and invasion to the level of untreated control group (Fig. 4E and 4F). A similar result was observed in the wound-healing assay after miR-486-3p overexpression reversed the effect of MDSCs (Fig. 4G and 4H).

miR-486-3p has been identified as a tumor suppressor associated with cancer cell proliferation and metastasis (27, 28). Furthermore, miR-486-3p has been reported to be significantly dysregulated in thyroid cancer compared

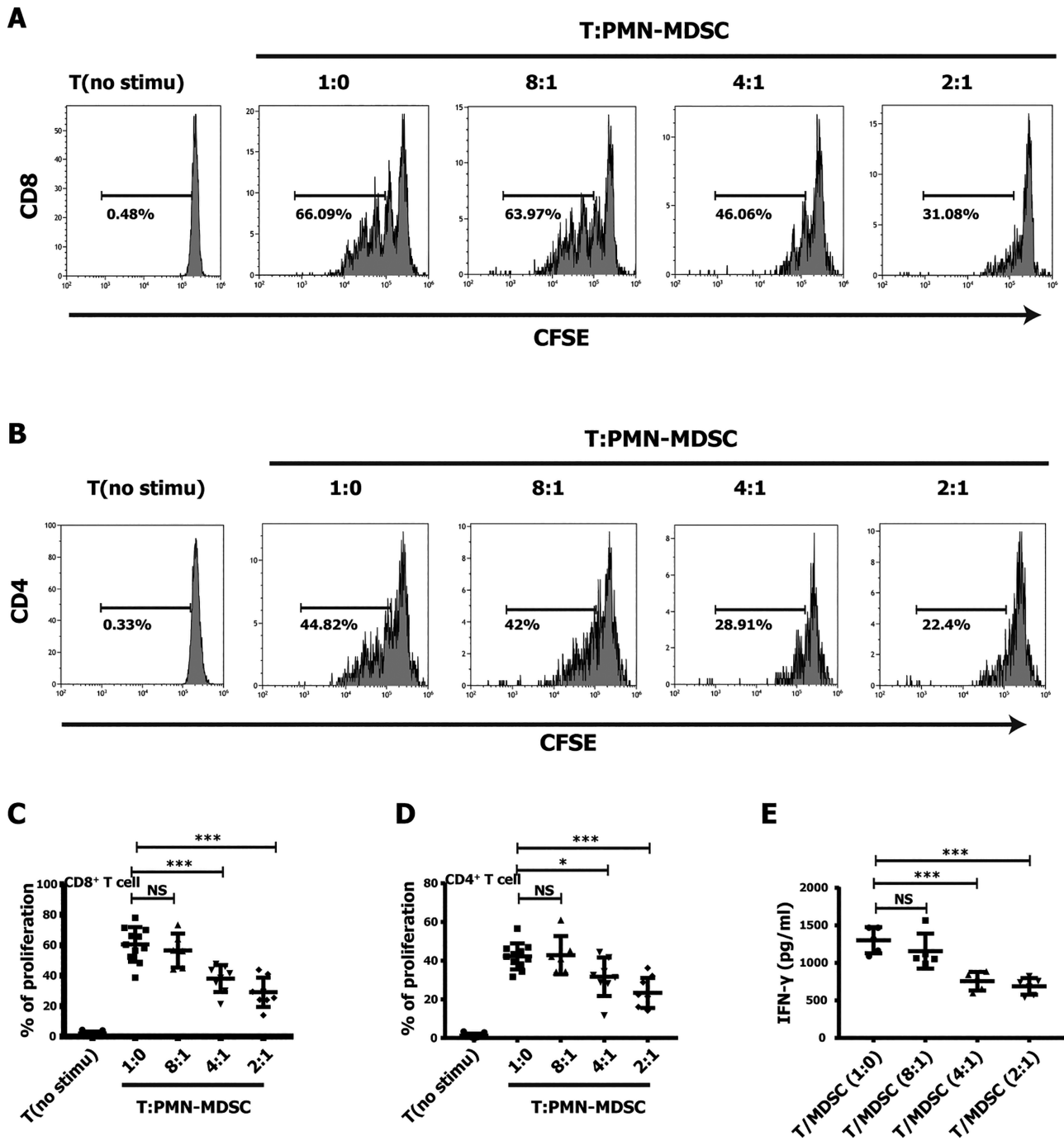


**Figure 2.** PMN-MDSCs from PTC patients suppress T-cell responses. CD3<sup>+</sup> T cells and PMN-MDSCs were sorted from the PBMC of PTC patients. (A, C) CD8<sup>+</sup> T cell proliferation and (B, D) CD4<sup>+</sup> T cell proliferation following stimulation with anti-CD3/CD28 antibodies in the presence or absence of PMN-MDSCs was measured by CFSE. (E) Production of IFN-γ was measured by enzyme-linked immunosorbent assay. For each sample preparation, CD3<sup>+</sup> T cells and PMN-MDSCs were isolated from the PBMC of the same PTC patients. No stimulation corresponds to T cells untreated with anti-CD3/CD28 antibodies. Data are presented as mean ± SD, \*P < .05, \*\*\*P < .001. NS, not significant.

with adjacent tissue (29). Transfection of miR-486-3p mimics decreased the number of migrated and invaded cells while addition of a miR-486-3p inhibitor led to opposite results (Fig. 5A and 5B). Tumor cells transfected with miR-486-3p inhibitor demonstrated elevated migratory ability by the wound-healing assay. In contrast, miR-486-3p overexpression caused a sharp

decrease in wound closure rates (Fig. 5C). In addition, overexpression of miR-486-3p inhibited proliferation of TPC-1 cells, while there was no significant difference in cell viability between the miR-486-3p inhibitor-treated and control groups (22).

Stable cell lines transduced with miR-486-3p and miR-486-3p inhibitor were established and injected

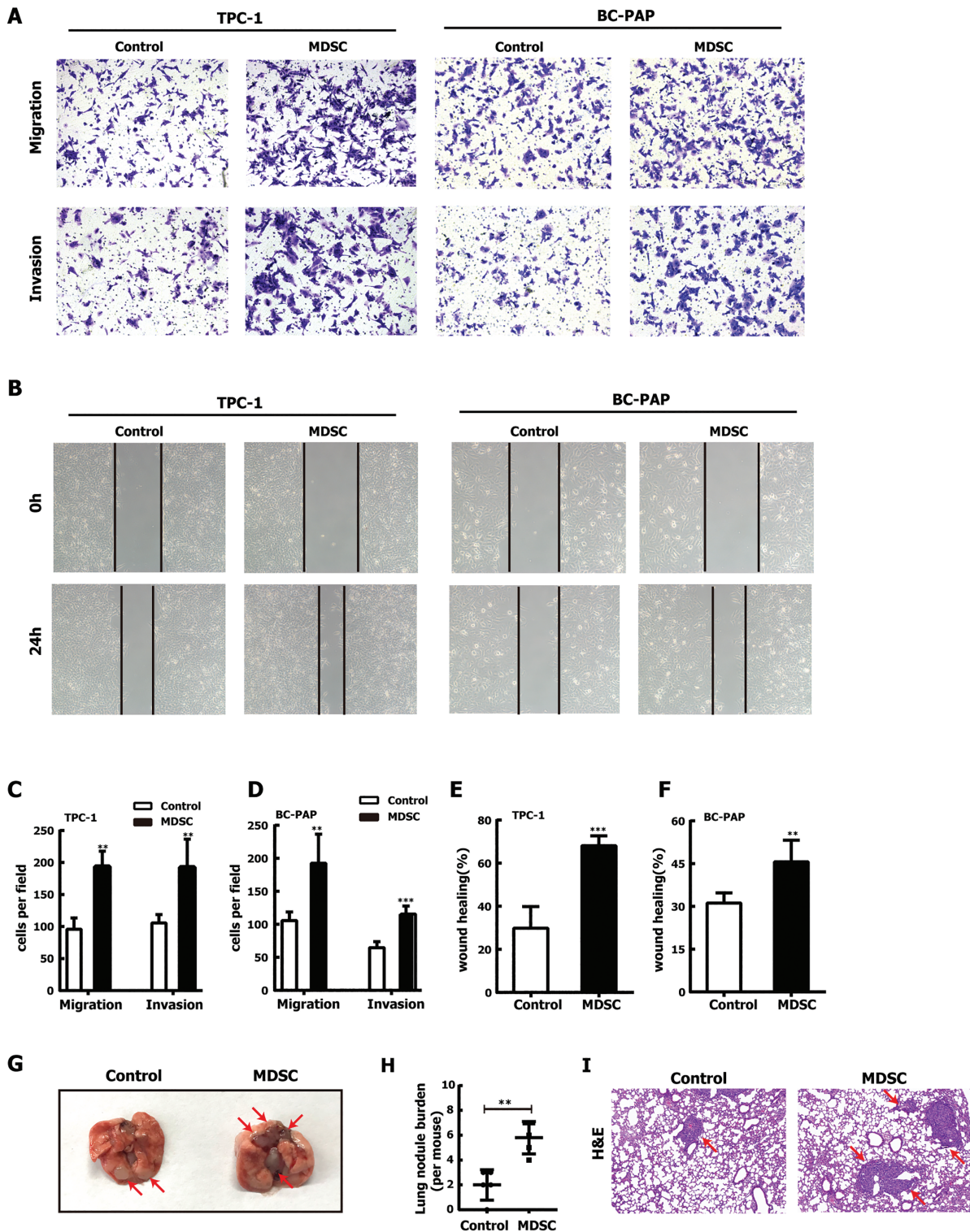


**Figure 3.** PMN-MDSCs enhance PTC cell migration and invasion. (A) Migration and invasion were measured by transwell assay in TPC-1 (n = 5) and BC-PAP (n = 4) cells co-cultured with or without PMN-MDSCs for 48 hours. (B) Wound-healing assay was performed to investigate cell migration ability in TPC-1 (n = 5) and BC-PAP (n = 5) cells co-cultured with or without PMN-MDSCs for 48 hours. (C, D) The number of migrated and invaded cells and (E, F) the area of migrated cells per low field was quantified. Data are shown from at least 3 patients and in triplicate. (G) Mice (n = 5) were intravenously injected with TPC-1 cells cocultured with or without PMN-MDSCs. Representative images of murine whole lungs are shown. Arrows indicate lung tumor nodules. (H) The number of visible tumor nodules was measured. (I) Representative H&E staining of lung tissues. Arrows indicate metastases (magnification,  $\times 100$ ). Data are presented as mean  $\pm$  SD, \*\* $P < .01$ , \*\*\* $P < .001$ .

into nude mice intravenously, respectively. Mice injected with TPC-1 cells overexpressing miR-486-3p exhibited reduced pulmonary metastasis while those injected with

TPC-1 cells stably expressing miR-486-3p inhibitor experienced significantly accelerated metastatic growth (Fig. 5D and 5E). Tumorigenic activity was confirmed

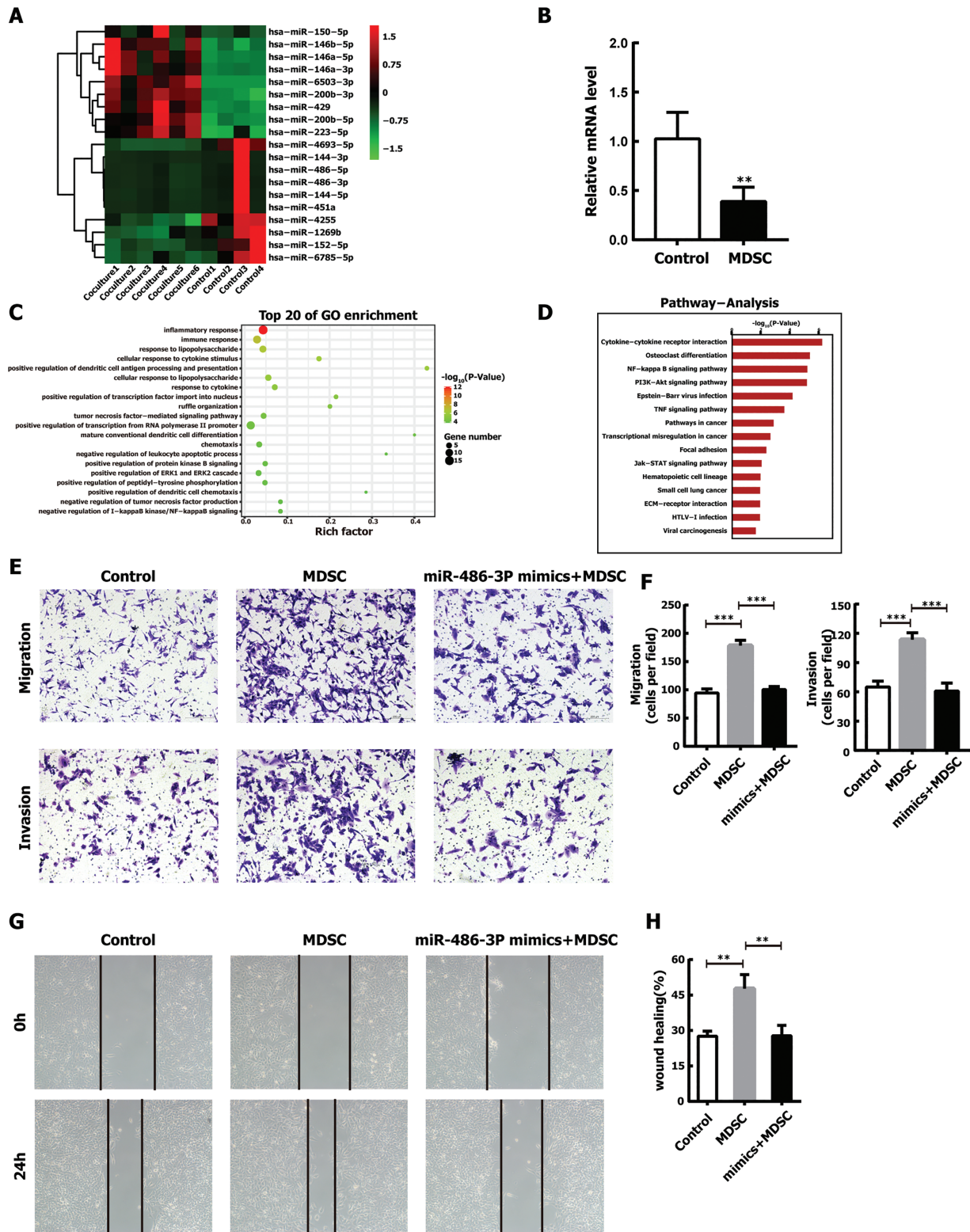


**Figure 4.** PMN-MDSCs promote cell migration and invasion via miR-486-3p downregulation. (A) miRNA microarray heatmap showing differentially expressed miRNAs between TPC-1 cells cocultured with and without PMN-MDSCs. Each vertical line (coculture 1-6) represents miRNA expression from TPC-1 tumor cells co-cultured with PMN-MDSCs from PBMC of one of 6 different patients. (B) Validation of miR-486-3p expression by qRT-PCR. (C, D) Genes targeted by the differentially expressed miRNAs, as identified by Top GO and KEGG pathway analysis. (E, F) TPC-1 cells were separated into three groups and cultured without any treatment (control); with sorted PMN-MDSCs from PTC patients (MDSC group); or with miR-486-3p mimics for 24 hours followed by culture with sorted PMN-MDSCs for another 48 hours (miR-486-3p mimics+MDSC group). Cell migration and invasion abilities were assessed by transwell assays. (G, H) Migration ability of each group of treated TPC-1 cells, as determined by wound-healing assay. Experiments were performed from at least three patients and in triplicate. Data are presented as mean  $\pm$  SD,  $**P < 0.01$ ,  $***P < 0.001$ .

histologically by H&E staining (Fig. 5F). Taken together, these data demonstrated that miR-486-3p functions as a tumor suppressor in thyroid cancer, and PMN-MDSCs accelerated invasion and metastasis, at least partially, by suppressing miR-486-3p.

### Effect of NF- $\kappa$ B2 on cell migration and invasion

We conducted RNA-seq analysis to compare the mRNA expression profile of MDSC-conditioned and untreated TPC-1 cells (Fig. 6A). GO analysis was applied to the differentially expressed genes. Inflammation related response was the most significantly enriched GO

term, while the TNF signaling pathway, cytokine–cytokine receptor interaction, NF- $\kappa$ B signaling pathway, and chemokine signaling pathway were among the most significantly enriched signaling pathways (Fig. 6B, 6C).

Because the NF- $\kappa$ B signaling pathway is widely recognized as an important contributor to cancer progression and the tumor-promoting effect of MDSCs (26, 30), NF- $\kappa$ B2 (p52/p100), a member of the transcription factor complex NF- $\kappa$ B family, was selected for further functional analysis in thyroid cancer. The expression of p100/p52 and RelB were significantly increased in TPC-1 cells cocultured with PMN-MDSCs by qRT-PCR

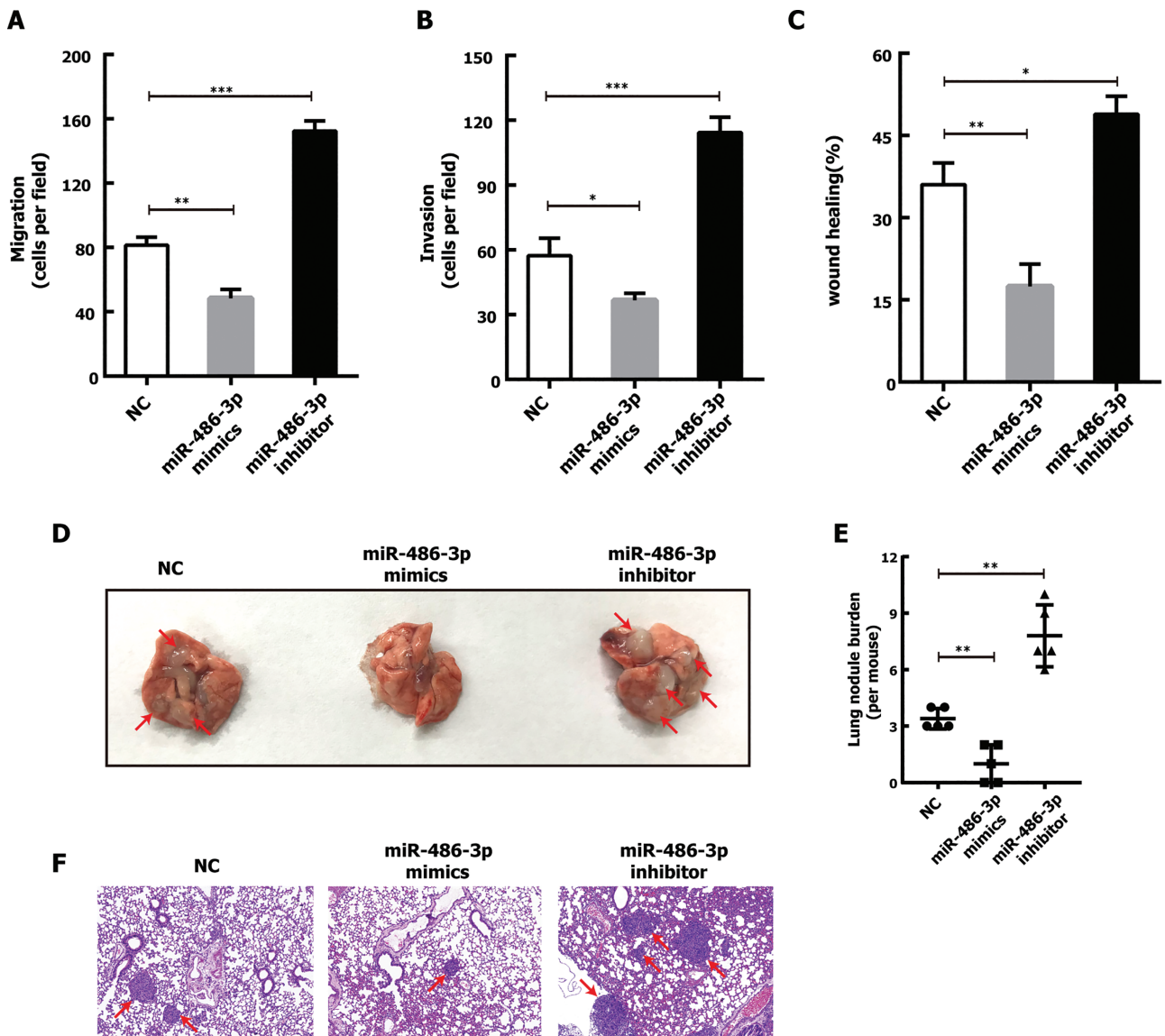


**Figure 5.** Effect of miR-486-3p on cell migration and invasion. (A, B) Migration and invasion of TPC-1 cells was examined by transwell assays after transfection with miR-486-3p mimics, miR-486-3p inhibitor or negative control. (C) Migration of TPC-1 cells was evaluated by wound-healing assay in each group. Experiments were performed in triplicates. (D) Representative images of murine whole lungs following tail vein injection of TPC-1 cell lines transfected with lentiviral vectors expressing miR-486-3p precursor, miR-486-3p inhibitor and the negative control miRNA sequences into nude mice. Five mice were used for each group. Arrows indicate lung nodules. (E) The numbers of lung tumor nodules in each group. (F) Representative images of H&E staining. Arrows indicate metastases (magnification,  $\times 100$ ). Data are presented as mean  $\pm$  SD, \* $P < .05$ , \*\* $P < .01$ , \*\*\* $P < .001$ .

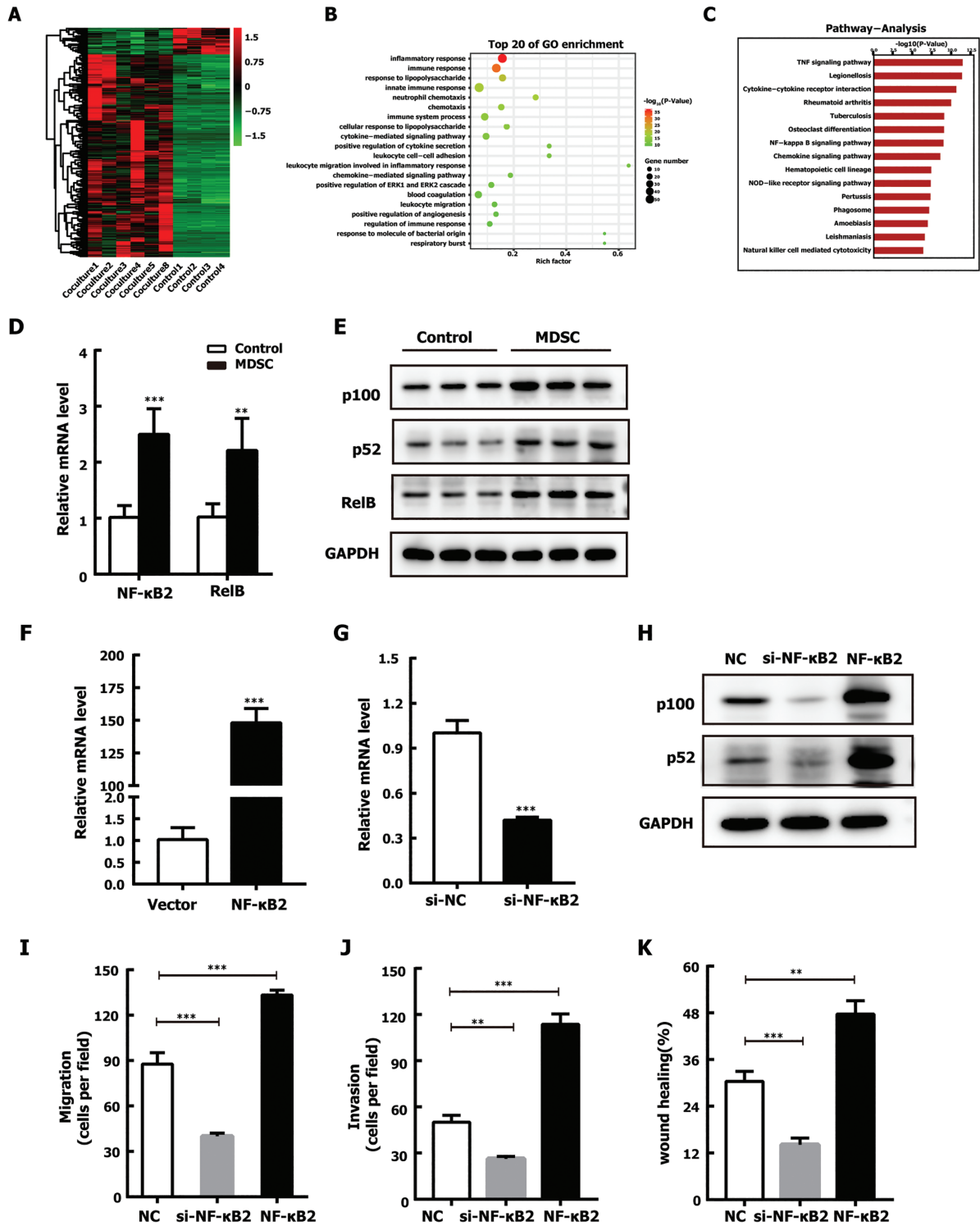


**Figure 6.** Effect of NF- $\kappa$ B2 on cell migration and invasion. (A) The expression profiles of TPC-1 cells co-cultured with and without PMN-MDSCs were compared by RNA-seq analysis. Heatmap demonstrates differentially expressed genes. Each vertical line (co-culture 1-6) represents tumor cells cocultured with PMN-MDSCs from PBMC of one of six different patients. (B) Top GO analysis identifying ontologies of differentially expressed mRNAs. (C) KEGG pathways corresponding to differentially expressed mRNAs. (D) qRT-PCR analysis of NF- $\kappa$ B2 and RelB in TPC-1 cells cultured with or without PMN-MDSCs. (E) Western blot analysis of NF- $\kappa$ B2 and RelB protein expression. Data from three patients in triplicates are shown. (F, G) qRT-PCR assay was conducted to evaluate the efficiency of overexpression or knockdown of NF- $\kappa$ B2 in TPC-1 cells transfected with siNF- $\kappa$ B2 or NF- $\kappa$ B2 vector. (H) Western blot analysis of NF- $\kappa$ B2 expression. (I, J) Transwell assay of TPC-1 cells. (K) Wound-healing assay of TPC-1 cells. Data from three experiments in triplicates are shown. Data are presented as mean  $\pm$  SD, \*\* $P < .01$ , \*\*\* $P < .001$ .

and Western blot analysis (Fig. 6D and 6E), confirming the RNA-seq findings.

We then explored the function of NF- $\kappa$ B2 in modulating migration and invasion capabilities of PTC by manipulating its expression by siRNA knockdown and gene overexpression in TPC-1 cells (Fig. 6F-6H). The results showed that NF- $\kappa$ B2 overexpression increased the motility and invasiveness of PTC cells, whereas cell migration and invasion diminished after NF- $\kappa$ B2 knockdown (Fig. 6I-6K). These results suggested that PMN-MDSCs-induced NF- $\kappa$ B2 overexpression promotes the migration and invasion of TPC-1 cells.

### PMN-MDSCs facilitate cell migration and invasion by regulating the miR-486-3p/NF- $\kappa$ B2 axis

To further elucidate the inhibitory role of miR-486-3p in PTC, miRNA target analysis was performed. Strikingly, NF- $\kappa$ B2 was also identified as a putative target gene using the Miranda and RNAhybrid databases, with predicted interactions between miR-486-3p and target sites on the NF- $\kappa$ B2 3'-UTR (Fig. 7A). To confirm whether miR-486-3p targets NF- $\kappa$ B2 directly, NF- $\kappa$ B2-WT and NF- $\kappa$ B2-Mut plasmids containing the NF- $\kappa$ B2 3' UTR fused to the luciferase gene were constructed. miR-486-3p expression significantly decreased luciferase activity of NF- $\kappa$ B2-WT, but not NF- $\kappa$ B2-Mut, in 293T cells, indicating a direct interaction between miR-486-3p and NF- $\kappa$ B2 via the 3' UTR (Fig. 7B).

Overexpression of miR-486-3p in TPC-1 cells suppressed the protein expression of p100/p52, whereas miR-486-3p inhibitor increased p100/p52 expression (Fig. 7C). TPC-1 cells cotransfected with NF- $\kappa$ B2 vector and miR-486-3p mimics demonstrated markedly decreased NF- $\kappa$ B2 levels compared with cells transfected with NF- $\kappa$ B2 vector alone (Fig. 7D).

We lastly explored the functional effects of overexpression of both NF- $\kappa$ B2 and miR-486-3p in TPC-1 cells to investigate whether miR-486-3p can hamper NF- $\kappa$ B2 driven PTC progression. We confirmed that enhanced migration of TPC-1 cells caused by PMN-MDSCs was attenuated by miR-486-3p mimics, while NF- $\kappa$ B2 overexpression reversed the inhibitory effects of miR-486-3p mimics. Similar results were observed in the invasion assay (Fig. 7E-7H). In conclusion, PMN-MDSCs promote PTC cell migration and invasion by suppressing miR-486-3p expression and consequently driving overexpression of NF- $\kappa$ B2.

## Discussion

MDSCs have been previously reported to be enriched in the blood of patients with colon cancer,

pancreatic cancer, non-small cell lung cancer, and even premalignant disease (31, 32). The population of circulating MDSCs correlates inversely with clinical stage and overall survival, showing that circulating MDSCs play an important role in tumor progression (32, 33). Previous studies showed that PMN-MDSCs are generally far more prevalent in tumors than M-MDSCs (8). This study is the first to report on the roles of MDSCs in regulating tumor progression in thyroid cancer. We confirmed the above findings in PTC cells, demonstrating a significant elevation of PMN-MDSCs but not M-MDSCs in the peripheral blood of PTC patients. Expansion of PMN-MDSCs was associated with several aggressive characteristics of PTC, including old age, tumor invasion, distant metastasis, and advanced tumor stage. Additionally, circulating PMN-MDSCs dampened T cell immune responses, in accordance with the standard functional definition of MDSCs (8). In aggregate, these findings suggest that circulating MDSCs may serve as a potential minimally biomarker for PTC diagnosis confirmation.

An understanding of how MDSCs facilitate cancer cell metastasis has only recently begun to emerge. MDSCs support metastasis through multiple mechanisms, including production of chemokines, cytokines and secreted enzymes, premetastatic niche preparation, and interaction with tumor cells (7, 8). Sprouse et al. demonstrated that circulating MDSCs directly interact with circulating tumor cells and in turn foster tumor-initiating capabilities (34). This study revealed that coculture of PMN-MDSCs with PTC cells increased tumor cell metastatic ability both in vitro and in vivo. With the help of miRNA profiling and RNA-seq, we helped confirm the hypothesis that PMN-MDSCs regulate tumor phenotype by modulating miRNAs and mRNA expression in cancer cells. We found that PMN-MDSCs repress the expression of miR-486-3p in PTC cells, leading to increased NF- $\kappa$ B2 expression. Furthermore, miR-486-3p restoration attenuated the effects of PMN-MDSCs on cell migration and invasion.

The NF- $\kappa$ B signaling pathway is a key mediator of MDSC activation in various cancer disease states. The canonical NF- $\kappa$ B pathway expands MDSC number through transforming growth factor beta in cancer models (35). Additionally, noncanonical NF- $\kappa$ B acts by mediating STAT3-stimulated indoleamine 2,3-dioxygenase upregulation to promote MDSC immunosuppressive functions in breast cancer (36). Both sides of the NF- $\kappa$ B signaling pathway likely also play a role in facilitating immune escape/tumor progression in PTC. Our results demonstrated that PMN-MDSCs cocultured with PTC cells induce NF- $\kappa$ B2 activation.

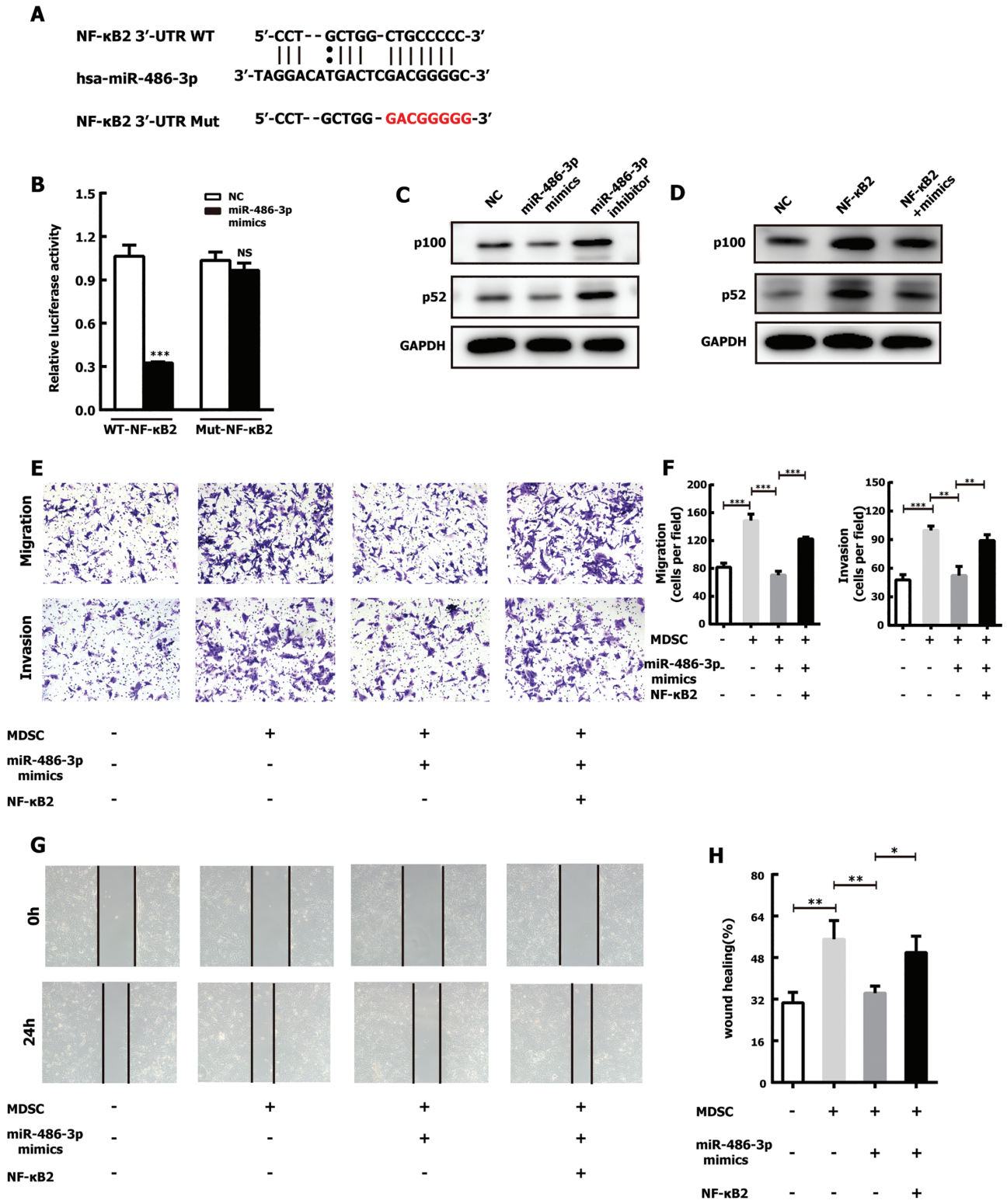


**Figure 7.** PMN-MDSCs facilitate cell migration and invasion by downregulating the miR-486-3p axis and upregulating NF-κB2. (A) Predicted binding sequences between miR-486-3p and NF-κB2. (B) Relative luciferase activity in 293T cells co-transfected with miR-NC/miR-486-3p mimics and NF-κB2-WT/ NF-κB2-Mut. (C) Western blot analysis of NF-κB2 expression in TPC-1 cells transfected with miR-486-3p mimics and miR-486-3p inhibitor. (D) Western blot analysis of NF-κB2 expression after TPC-1 cells were transfected with miR-486-3p mimics or cotransfected with miR-486-3p mimics and NF-κB2 vector. Experiments were performed in triplicate. (E, F) The ability of migration and invasion was evaluated by transwell assay in TPC-1 cells transfected with miR-486-3p mimics or co-transfected with miR-486-3p mimics and NF-κB2 vector, cultured with or without PMN-MDSCs. (G, H) Wound-healing assays were performed for each group on at least three patients and in triplicate. Data are presented as mean ± SD, \**P* < .05, \*\**P* < .01, \*\*\**P* < .001.

Moreover, upregulation of NF- $\kappa$ B2 leads to accelerated migration and invasion of PTC cells in vitro. Finally, we confirmed that NF- $\kappa$ B2 is activated in MDSC-conditioned cancer cells and that miR-486-3p directly downregulates the NF- $\kappa$ B2 transcript via its 3' UTR.

There are 2 limitations in the present study. First, the number of patients with distant metastasis and advanced stage is small; this may be attributed to the fact that most thyroid cancer cases were diagnosed at the early stage in recent years. Our finding, PMN-MDSCs are associated with distant metastasis and advanced tumor stage, needs to be confirmed in further studies that have enrolled a large number of PTC cases. Second, although we found that miR-486-3p and its downstream target NF- $\kappa$ B2 played a key role in mediating the function of MDSCs in PTC, how MDSCs induced the dysregulation of miR-486-3p was not explored. Based on the previous finding that MDSC is capable of secreting high levels of cytokines (8) and these cytokines downregulate miRNA expression (37, 38), it is reasonable to assume that MDSC-released cytokines account for the repression of miR-486-3p, which needs to be further confirmed.

Taken together, our data demonstrated that PMN-MDSCs regulate PTC cell metastasis by downregulating miR-486-3p and that NF- $\kappa$ B2 is a primary target gene of miR-486-3p in the PTC context. Blocking PMN-MDSCs and inducing miR-486-3p expression may represent potential therapeutic approaches in PTC.

## Acknowledgments

We are grateful to Prof. Haixia Guan (The First Affiliated Hospital of China Medical University) for the gift of BC-PAP and TPC-1 cells.

**Financial Support:** This work was supported by grants from the National Natural Science Foundation of China (81702648 and 81772850) and National Key Research and Development Program of China (2018YFC1314100).

## Additional Information

**Correspondence and Reprint Requests:** Haipeng Xiao, MD, PhD, Department of Endocrinology, The First Affiliated Hospital, Sun Yat-Sen University, 58 Zhongshan Road #2, Guangzhou, Guangdong 510080, China. E-mail: [xiaohp@mail.sysu.edu.cn](mailto:xiaohp@mail.sysu.edu.cn); or Shuang Yu, MD, PhD, Department of Endocrinology, The First Affiliated Hospital, Sun Yat-Sen University, 58 Zhongshan Road #2, Guangzhou, Guangdong 510080, China. E-mail: [shuang.yu@aliyun.com](mailto:shuang.yu@aliyun.com).

**Disclosure Summary:** The authors report nothing to declare. No competing financial interests exist.

**Data Availability:** All data generated or analyzed during this study are included in this published article or in the data repositories listed in References.

## References

- Cabanillas ME, McFadden DG, Durante C. Thyroid cancer. *Lancet*. 2016;388(10061):2783-2795.
- Roman BR, Morris LG, Davies L. The thyroid cancer epidemic, 2017 perspective. *Curr Opin Endocrinol Diabetes Obes*. 2017;24(5):332-336.
- Sancho JJ, Lennard TW, Paunovic I, Triponez F, Sitges-Serra A. Prophylactic central neck dissection in papillary thyroid cancer: a consensus report of the European Society of Endocrine Surgeons (ESES). *Langenbecks Arch Surg*. 2014;399(2):155-163.
- Lundgren CI, Hall P, Dickman PW, Zedenius J. Clinically significant prognostic factors for differentiated thyroid carcinoma: a population-based, nested case-control study. *Cancer*. 2006;106(3):524-531.
- Wu T, Dai Y. Tumor microenvironment and therapeutic response. *Cancer Lett*. 2017;387(28):61-68.
- Hui L, Chen Y. Tumor microenvironment: sanctuary of the devil. *Cancer Lett*. 2015;368(1):7-13.
- Marvel D, Gabrilovich DI. Myeloid-derived suppressor cells in the tumor microenvironment: expect the unexpected. *J Clin Invest*. 2015;125(9):3356-3364.
- Bronte V, Brandau S, Chen SH, et al. Recommendations for myeloid-derived suppressor cell nomenclature and characterization standards. *Nat Commun*. 2016;7:12150.
- Talmadge JE, Gabrilovich DI. History of myeloid-derived suppressor cells. *Nat Rev Cancer*. 2013;13(10):739-752.
- Shen P, Wang A, He M, Wang Q, Zheng S. Increased circulating Lin(-/low) CD33(+) HLA-DR(-) myeloid-derived suppressor cells in hepatocellular carcinoma patients. *Hepatol Res*. 2014;44(6):639-650.
- Yu J, Du W, Yan F, et al. Myeloid-derived suppressor cells suppress antitumor immune responses through IDO expression and correlate with lymph node metastasis in patients with breast cancer. *J Immunol*. 2013;190(7):3783-3797.
- Cui TX, Kryczek I, Zhao L, et al. Myeloid-derived suppressor cells enhance stemness of cancer cells by inducing microRNA101 and suppressing the corepressor CtBP2. *Immunity*. 2013;39(3):611-621.
- Panni RZ, Sanford DE, Belt BA, et al. Tumor-induced STAT3 activation in monocytic myeloid-derived suppressor cells enhances stemness and mesenchymal properties in human pancreatic cancer. *Cancer Immunol Immunother*. 2014;63(5):513-528.
- Angell TE, Lechner MG, Smith AM, et al. Circulating myeloid-derived suppressor cells predict differentiated thyroid cancer diagnosis and extent. *Thyroid*. 2016;26(3):381-389.
- Gunda V, Gigliotti B, Ashry T, et al. Anti-PD-1/PD-L1 therapy augments lenvatinib's efficacy by favorably altering the immune microenvironment of murine anaplastic thyroid cancer. *Int J Cancer*. 2019;144(9):2266-2278.
- Gunda V, Gigliotti B, Ndishabandi D, et al. Combinations of BRAF inhibitor and anti-PD-1/PD-L1 antibody improve survival and tumour immunity in an immunocompetent model of orthotopic murine anaplastic thyroid cancer. *Br J Cancer*. 2018;119(10):1223-1232.
- El Gazzar M. microRNAs as potential regulators of myeloid-derived suppressor cell expansion. *Innate Immun*. 2014;20(3):227-238.
- Safarzadeh E, Orangi M, Mohammadi H, Babaie F, Baradaran B. Myeloid-derived suppressor cells: Important contributors to tumor progression and metastasis. *J Cell Physiol*. 2018;233(4):3024-3036.
- Deng Z, Rong Y, Teng Y, et al. Exosomes miR-126a released from MDSC induced by DOX treatment promotes lung metastasis. *Oncogene*. 2017;36(5):639-651.

20. DeLellis RA, Lloyd RV, Heitz PU, Eng C. *WHO Classification of Tumours. Pathology and Genetics of Tumours of Endocrine Organs*. Lyon, France: IARC Press; 2004.
21. Draghici S, Khatri P, Tarca AL, et al. A systems biology approach for pathway level analysis. *Genome Res*. 2007;17(10):1537-1545.
22. Chen L, Xiong L, Hong S, et al. Supplemental data for “Circulating myeloid-derived suppressor cells facilitate invasion of thyroid cancer cells by repressing miR-486-3p.” *Dryad* Dataset. 2020. Deposited 19 April 2020. <https://datadryad.org/stash/share/59S9DohUGGT444jt84hnsCxTQoD8rqXunWRsI8-G7IU>.
23. Kursunel MA, Esendagli G. The untold story of IFN- $\gamma$  in cancer biology. *Cytokine Growth Factor Rev*. 2016;31:73-81.
24. Chan SH, Wang LH. Regulation of cancer metastasis by microRNAs. *J Biomed Sci*. 2015;22(1):9.
25. Khan AQ, Ahmed EI, Elareer NR, Junejo K, Steinhoff M, Uddin S. Role of miRNA-regulated cancer stem cells in the pathogenesis of human malignancies. *Cells* 2019;8(8):840.
26. Gabrilovich DI, Nagaraj S. Myeloid-derived suppressor cells as regulators of the immune system. *Nat Rev Immunol*. 2009;9(3):162-174.
27. Chou ST, Peng HY, Mo KC, et al. MicroRNA-486-3p functions as a tumor suppressor in oral cancer by targeting DDR1. *J Exp Clin Cancer Res*. 2019;38(1):281.
28. Ye H, Yu X, Xia J, Tang X, Tang L, Chen F. MiR-486-3p targeting ECM1 represses cell proliferation and metastasis in cervical cancer. *Biomed Pharmacother*. 2016;80:109-114.
29. Swierniak M, Wojcicka A, Czetwertynska M, et al. In-depth characterization of the microRNA transcriptome in normal thyroid and papillary thyroid carcinoma. *J Clin Endocrinol Metab*. 2013;98(8):E1401-E1409.
30. Hoesel B, Schmid JA. The complexity of NF- $\kappa$ B signaling in inflammation and cancer. *Mol Cancer*. 2013;12:86.
31. Ma P, Beatty PL, McKolanis J, Brand R, Schoen RE, Finn OJ. Circulating Myeloid Derived Suppressor Cells (MDSC) that accumulate in premalignancy share phenotypic and functional characteristics with MDSC in cancer. *Front Immunol*. 2019;10:1401.
32. Barrera L, Montes-Servín E, Hernandez-Martinez JM, et al. Levels of peripheral blood polymorphonuclear myeloid-derived suppressor cells and selected cytokines are potentially prognostic of disease progression for patients with non-small cell lung cancer. *Cancer Immunol Immunother*. 2018;67(9):1393-1406.
33. Diaz-Montero CM, Finke J, Montero AJ. Myeloid-derived suppressor cells in cancer: therapeutic, predictive, and prognostic implications. *Semin Oncol*. 2014;41(2):174-184.
34. Sprouse ML, Welte T, Boral D, et al. PMN-MDSCs Enhance CTC Metastatic Properties through Reciprocal Interactions via ROS/Notch/Nodal Signaling. *Int J Mol Sci*. 2019;20(8):1916.
35. Wang DJ, Ratnam NM, Byrd JC, Guttridge DC. NF- $\kappa$ B functions in tumor initiation by suppressing the surveillance of both innate and adaptive immune cells. *Cell Rep*. 2014;9(1):90-103.
36. Yu J, Wang Y, Yan F, et al. Noncanonical NF- $\kappa$ B activation mediates STAT3-stimulated IDO upregulation in myeloid-derived suppressor cells in breast cancer. *J Immunol*. 2014;193(5):2574-2586.
37. Bandini E, Rossi T, Gallerani G, Fabbri F. Adipocytes and microRNAs crosstalk: a key tile in the mosaic of breast cancer microenvironment. *Cancers* 2019;11(10):1451.
38. Yin Y, Yao S, Hu Y, et al. The immune-microenvironment confers chemoresistance of colorectal cancer through macrophage-derived IL6. *Clin Cancer Res*. 2017;23(23):7375-7387.